Manifestations of Nonlocal Exchange, Correlation, and Dynamic Effects in X-Ray Scattering

M. Jung, R. W. Dunford, D. S. Gemmell, E. P. Kanter, B. Krässig, T. W. LeBrun, S. H. Southworth, and L. Young
Physics Division, Argonne National Laboratory, Argonne, Illinois 60439

J. P. J. Carney, L. LaJohn, and R. H. Pratt
Department of Physics and Astronomy, University of Pittsburgh, Pittsburgh, Pennsylvania 15260

P. M. Bergstrom, Jr.
N Division, Lawrence Livermore National Laboratory, Livermore, California 94551
(Received 13 April 1998)

We report precise measurements of differential x-ray scattering cross sections in Ne and He from 11–22 keV and develop a method for obtaining predictions of comparable accuracy (1%). The measurement of ratios (total scattering in Ne to He and Compton to Rayleigh scattering in Ne) facilitates comparison to theories. We find evidence for the need to include nonlocal exchange, electron correlation, and dynamic effects for an accurate description at low Z and conclude that no single current theory is sufficient. [S0031-9007(98)06921-X]

PACS numbers: 32.80.Cy, 07.85.–m

The use of x rays has been of fundamental importance in a number of fields, from demonstrating the validity of the quantum theory of radiation [1] to determining macromolecular structures such as DNA [2]. Recent advances in experimental techniques, such as the use of modern synchrotron sources that permit accurate experiments with well-defined initial conditions, coupled with similar advances in theory, such as the development of computer codes that calculate the relativistic S-matrix, now make it possible to perform precision investigations necessary to probe details in the description of atomic x-ray scattering. Among the phenomena that have recently been investigated are the need for multipoles in describing photon-atom interactions [3] and the effects of electron correlations on atomic processes ([4], and references therein). In this Letter we describe the need for nonlocal effects in describing x-ray scattering, even at relatively high energies, and confirm the need for inclusion of electron correlation and dynamic effects. In obtaining these results, we performed the first experimental decomposition of Compton scattering from Rayleigh scattering in free atoms. We also describe experimental and theoretical methods to obtain absolute scattering cross sections at an accuracy of $\approx 1\%$. Our results have broad implications for calculations of elastic and inelastic photon scattering from light elements, which are widely used to determine crystallographic structures and electron momentum distributions.

Relativistic S-matrix calculations of elastic photon scattering have been available for some time [5]. These have mainly been tested by high energy x- or γ-ray scattering on solid targets composed of heavy elements [6] where they are superior to other, simpler techniques, leading to their wide acceptance as a benchmark [7]. Only recently [8] has a similar theory been successfully applied to Compton scattering. This theory has not been as extensively tested against measurements. In both cases, the emphasis has been on an accurate description of the photon-atom interaction. The main approximations are made in the description of the atom, which is assumed to be spherically symmetric and with the electron-electron interactions included only within the independent particle (IPA) and local exchange approximations.

Simpler predictions for these cross sections can be obtained by calculating form factors (FF) for Rayleigh scattering, and Compton profiles, using the impulse approximation (IA), and incoherent scattering factors [(ISF), which include the Raman channel] for Compton scattering. These theories are derived from the A^2 term of the nonrelativistic Hamiltonian [$H_{\rm int} = (1/2mc^2)e^2A^2 - (e/mc)\mathbf{p} \cdot \mathbf{A}$]. Such calculations can be performed using bound state wave functions in a nonrelativistic local central potential (e.g., FF [9] calculated using Hartree-Fock-Slater wave functions [10]), or with greater sophistication for the relativistic case (modified form factor, MFF [11]), or including effects which go beyond the IPA. Examples are the nonrelativistic [12] and relativistic [13] nonlocal FF and ISF of Hubbell *et al.* Beyond the IPA, some results for FF and ISF exist [14–16]. Other corrections include the anomalous scattering factor (ASF) for Rayleigh scattering and the coherent nuclear Thomson (NT) amplitude.

Very few experiments have been reported for scattering from free atoms [17–20], the case for which cross sections are usually calculated. In view of the basic need for accurate and absolute measurements in free atoms to assess the importance of various approximations, we have explored scattering from neon at 90° in the 11 to 22 keV range where sizable differences (up to 16%) between the S-matrix and nonlocal exchange form-factor calculations of the elastic scattering channel exist. As described below,

 0031-9007/98/81(8)/1596(4)$15.00

the major source of the difference in light elements can be traced to the local exchange approximation with additional important contributions arising from electron correlation and dynamic effects.

We measured polarization-independent differential cross sections in Ne at energies far above the K edge (870 eV) and where Compton and Rayleigh scattering cross sections are comparable. By measuring ratios, $d\sigma_{\rm tot}({\rm Ne})/d\sigma_{\rm tot}({\rm He})$ and $d\sigma_C({\rm Ne})/d\sigma_R({\rm Ne})$, several difficult *absolute* measurements were circumvented, e.g., of x-ray flux and detector efficiency, and it was thus possible to obtain high accuracy. (In this paper, $d\sigma_{\rm tot}, d\sigma_C, d\sigma_R$ denote differential cross sections at 90° for total, Compton, and Rayleigh scattering, respectively, and $d\sigma_{\rm tot} = d\sigma_C + d\sigma_R$). The ratio of total scattering in Ne to He is a good test of theory because the He total scattering cross sections are well described by nonrelativistic, nonlocal ISF [12] over this energy and momentum transfer range.

The experiment was performed on a bending magnet beam line (12BM) at the Basic Energy Sciences Synchroton Radiation Center (BESSRC) of the Advanced Photon Source. Monochromatic x rays ($\Delta E/E \approx 1.4 \times 10^{-4}$) created a line source in the gas target which was viewed simultaneously by two well-characterized Si(Li) detectors [21] placed orthogonal to each other and to the photon beam propagation axis. Polarization-independent cross sections are obtained for any polarization state of the incident beam by averaging the yield in the above geometry. The detector acceptances were defined by two apertures and determined though simulation to be $\approx 90° \pm 3°$. Scattered x rays passed through $\approx$25.4 mm of gas and a 125-μ Kapton window to the detectors. Gas pressure was measured to $\approx$0.25%. The higher harmonics of the incident beam entered only indirectly through run-to-run normalization, where the use of a low-Z gas (N_2) in the ion chambers decreased their contributions to $<$0.7%.

Measurements were made at 11, 15, 18, and 22 keV x-ray energies, and two pressures ($\approx$1 and 2 atm) for each gas, Ne and He. Background measurements, Fig. 1(a), taken with an evacuated cell, show no scattered light at the incident energy (in this case 22 keV). The two features at $\approx$24 and 25 keV correspond to K_α emission from In and Sb impurities in the detector. Backgrounds at the other energies were very similar in shape. The backgrounds were scaled and subtracted from the experimental spectra to produce the spectra shown in Figs. 1(b) and 1(c).

The normalized total differential scattering cross section was obtained via $d\sigma/d\Omega \propto [Y_a + Y_b]/[I_{00} N F_{\rm exit}]$. $Y_{a,b}$ are the integrated yields (for detectors "a" and "b") corrected for electronic live time. $I_{00} = (I_0 - I_{\rm bkg}\Delta T)F_{\rm inc}$ with I_0 = integral ion chamber current, $I_{\rm bkg}$ = dark count rate, and ΔT = the duration of the run. N is gas density and $F_{\rm inc}$ ($F_{\rm exit}$) = x-ray transmission to the interaction region (detectors). Extrapolation from the value measured at 1 atm to zero pressure provides corrections

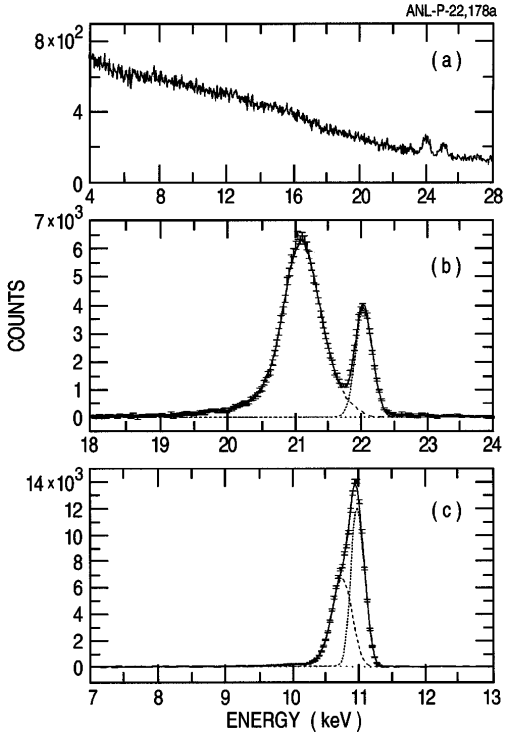

FIG. 1. Energy spectra in the Si(Li) detector oriented normal to the polarization plane. (a) Background spectrum with empty cell, (b) scattering from Ne at 22 keV, and (c) scattering from Ne at 11 keV. For (b) and (c) decomposition of the Compton and Rayleigh cross sections is shown in the dashed lines.

of $\approx$2% to the Ne cross sections. The He data exhibit no pressure-dependent effects. The experimental ratios, $d\sigma_{\rm tot}({\rm Ne})/d\sigma_{\rm tot}({\rm He})$, are shown in Fig. 2 and Table I. The experimental statistical errors are $\approx$0.2%. Systematic errors include (1) variations in background $\approx$0.2%, (2) extrapolation to zero pressure $\approx$0.4%, and (3) run-to-run variation in He normalization $\approx$0.7%. The latter is consistent with x-ray beam movement of $\approx \pm 0.5$ mm.

The Compton and Rayleigh cross sections were separated using the well-characterized detector response [21] and the IA Hartree-Fock Compton profiles [22]. The whole-atom profile was computed as the sum of the $1s$, $2s, 2p$ subshell profiles and was then used with the detector response to generate a Compton line shape. The amplitudes and positions of the generated Compton and Rayleigh line shapes were varied in a four-parameter fit to the experimental data. Examples of these fits are shown in Figs. 1(b) and 1(c). While the overlap between Compton and Rayleigh scattering is substantial at 11 keV, the separation is reliable to $\approx$8%. The uncertainty in $d\sigma_C({\rm Ne})/d\sigma_R({\rm Ne})$ decreases to $\approx$2% at 22 keV. These errors represent the sum of the fitting uncertainty ($\approx$2%) and the dispersion obtained from fits where the weights for the individual subshell IA profiles were unconstrained and the parameters describing the detector response were varied within uncertainties established by radioactive

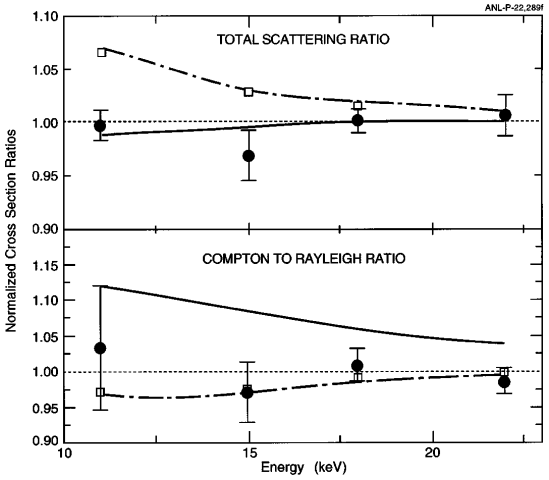

FIG. 2. Top: Ratio of total scattering cross section in neon to helium normalized to the "best" prediction (see text for description of best prediction). Bottom: Compton to Rayleigh cross section ratio in neon normalized to the best prediction for that ratio. Experiment (filled circles); Hubbell [12] (solid line); the most sophisticated theory for which comprehensive tabulations are currently available (MFF + ASF for Rayleigh, Hubbell [12] for Compton) (dot-dashed line). Squares show S-matrix Rayleigh and agreement with MFF + ASF results.

source measurements, He Compton profile fits, and Rayleigh line shapes in the Ne scattering spectra. Within this resolution, Raman scattering from the K (L) shell is included with the Compton (Rayleigh) cross section.

Table I shows experimental and theoretical values for the ratio of total scattering in Ne to He and the Ne Compton to Rayleigh ratio. The theoretical cross sections for 90° are used since the weighted average over the field of view ($90 \pm 3°$) is identical to $\approx 10^{-3}$. He cross sections are from Hubbell *et al.* [12]. The two columns following the experimental result show widely available theoretical results: simple scattering factors from Hubbell *et al.* [12] and the most sophisticated theory for which comprehensive tabulations are currently available (MFF + ASF [23] for Rayleigh, Hubbell *et al.* [12] for Compton). Figure 2 displays the experimental and theoretical results. Note in the top panel (total scattering cross section) that Hubbell's results are in good agreement with experiment, in contrast to the bottom panel (Compton to Rayleigh ratio). The opposite is true for the sophisticated MFF + ASF and S-matrix results.

The contradiction is resolved by examining the approximations made in these theories. The "simplest" predictions (Table I, column 6) are obtained from the form factor and impulse approximations, respectively (using local nonrelativistic IPA bound state wave functions and including the elastic NT amplitude). The best predictions (Table I, column 5) are composite results obtained by correcting the simplest for five effects (nonlocal exchange, electron correlation, relativity, dynamics, and Raman scattering). These effects are estimated by considering the various results within the FF, ISF, and IA approximations and by going beyond IA (Compton) and FF (Rayleigh). A perturbative regime is assumed in which all corrections are small and can be added linearly.

Table II shows percentage corrections for our situation. Nonlocal exchange corrections are obtained by comparing the nonlocal FF and ISF of Hubbell *et al.* [12] with local potential results; electron correlation effects by comparing the correlated FF and ISF of Wang *et al.* [14] with Hubbell *et al.* [12], and relativistic effects by comparing relativistic and nonrelativistic FF and IA calculations. Dynamic effects in the Rayleigh case are given by the ASF or S-matrix and in the Compton case by a comparison of relativistic IA, S-matrix, and exact A^2 calculations performed in a common screened central potential, as well as the contribution arising from the $\mathbf{p} \cdot \mathbf{A}$ terms [24] and for the difference between IA and A^2 calculations [25]. Their complex behavior reflects the portion of the Compton peak which is kinematically allowed in a given subshell at a given energy. Raman scattering is given by the A^2 calculations.

These corrections provide insight into the results given in Table I. In total scattering the corrections are additive

TABLE I. Comparison of experiment and theory. (i) Ratio of total scattering cross sections at 90° in Ne to He, $d\sigma_{\rm tot}({\rm Ne})/d\sigma_{\rm tot}({\rm He})$. (ii) Compton to Rayleigh ratio in Ne, $d\sigma_C({\rm Ne})/d\sigma_R({\rm Ne})$. The theoretical value of $d\sigma_{\rm tot}({\rm He})$ is from Hubbell *et al.* [12]. The headers for columns 3, 4 show the origin of the Rayleigh cross section (upper) and Compton cross section (lower). Best and simplest theoretical predictions are composite results as described in the text.

E		Hubbell	MFF + ASF		
(keV)	Expt.	Hubbell	Hubbell	Best	Simplest
		(i) $d\sigma_{\rm tot}({\rm Ne})/d\sigma_{\rm tot}({\rm He})$			
11	7.31 (10)	7.25	7.83	7.33	7.59
15	5.74 (14)	5.89	6.10	5.92	5.94
18	5.61 (6)	5.60	5.70	5.60	5.58
22	5.49 (10)	5.45	5.50	5.45	5.44
		(ii) $d\sigma_C({\rm Ne})/d\sigma_R({\rm Ne})$			
11	0.95 (8)	1.03	0.89	0.92	0.91
15	2.06 (9)	2.30	2.06	2.12	2.07
18	3.06 (7)	3.21	2.98	3.03	3.01
22	4.09 (8)	4.30	4.10	4.14	4.19

TABLE II. Percentage corrections for (i) Compton and (ii) Rayleigh scattering cross sections in neon for effects beyond the (i) impulse and (ii) form factor approximations (using local nonrelativistic IPA bound state wave functions). The additional effects are nonlocal—use of a nonlocal potential; electron correlation (Cor.)—use of correlated wave functions beyond Hartree-Fock; relativistic (Rel.)—use of relativistic wave functions and modified form factor; dynamic (Dyn.)—going beyond the form factor (Rayleigh) or impulse (Compton) approximation; Raman effects (K and L-shell Raman processes appear with Compton and Rayleigh cross sections, respectively).

	(i) Compton					(ii) Rayleigh				
E (keV)	Nonlocal	Cor.	Rel.	Dyn.	Raman K shell	Nonlocal	Cor.	Rel.	Dyn.	Raman L shell
11	1.4%	−3.3%	−0.1%	−1.2%	0.0%	−9.5%	0.9%	−0.2%	4.8%	0.2%
15	1.1%	−1.0%	−0.1%	0.4%	0.0%	−6.2%	0.9%	−0.4%	3.9%	0.2%
18	0.9%	−0.4%	−0.1%	0.2%	0.0%	−3.3%	0.4%	−0.4%	3.3%	0.1%
22	0.7%	−0.2%	−0.1%	−0.6%	0.0%	−1.2%	0.1%	−0.5%	2.6%	0.1%

and can be significant. The simplest prediction does not do well at 11 keV. In the ratio of Compton to Rayleigh cross sections, however, it is the difference between the Compton and Rayleigh corrections that matter, giving rise to a rough cancellation, so that the best and simplest predictions are more in agreement. Neither Hubbell's tabulation nor the MFF + ASF prediction do well in both situations at all four energies.

In conclusion, none of the current theories for which numerical values are available can alone properly describe x-ray scattering in neon (and presumably in other light elements). The size of the dynamic effects indicates a need to go beyond the form factor (Rayleigh) and impulse (Compton) approximations to obtain accurate cross sections. While the current IPA S-matrix theories for Rayleigh and Compton scattering are known to work well for high-Z elements and high energies, for low Z they are less reliable because they do not include nonlocal exchange and electron correlation effects. As seen here, it is possible to correct existing calculations for the various effects and achieve accuracies at $\approx 1\%-2\%$ level in agreement with experiment.

We are indebted to M. Inokuti and R. Bonham for valuable discussions. We thank C. Kurtz, B. Zabransky, and the BESSRC staff (M. Beno, M. Engbretson, G. Jennings, G. Knapp, P. A. Montano, and C. Wiley) for assistance with the experiment and the U.S. Department of Energy, Office of Basic Energy Sciences under Contract No. W-31-109-ENG-38 for support. The work of P. M. B. is currently performed under the auspices of the U.S. Department of Energy under Contract No. W-7405-ENG-48.

[1] A. H. Compton, Phys. Rev. **21**, 483 (1923).
[2] J. D. Watson and F. H. C. Crick, Nature (London) **171**, 737 (1953).
[3] B. Krässig *et al.*, Phys. Rev. Lett. **75**, 4736 (1995).
[4] L. Spielberger *et al.*, Phys. Rev. Lett. **76**, 4685 (1996).
[5] G. E. Brown, R. E. Peierls, and J. B. Woodward, Proc. R. Soc. London A **227**, 51 (1955); W. R. Johnson and F. D. Feiock, Phys. Rev. **168**, 22 (1968); L. Kissel, R. H. Pratt, and S. C. Roy, Phys. Rev. A **22**, 1970 (1980).
[6] P. P. Kane, L. Kissel, R. H. Pratt, and S. C. Roy, Phys. Rep. **140**, 75 (1986).
[7] L. Kissel, B. Zhou, S. C. Roy, S. K. Sen Gupta, and R. H. Pratt, Acta Crystallogr. Sect. A **51**, 271 (1995).
[8] T. Suric, P. M. Bergstrom, Jr., K. Pisk, and R. H. Pratt, Phys. Rev. Lett. **67**, 189 (1991); P. M. Bergstrom, Jr., T. Suric, K. Pisk, and R. H. Pratt, Phys. Rev. A **48**, 1134 (1993).
[9] H. P. Hanson, F. Herman, J. D. Lea, and S. Skillman, Acta Crystallogr. **17**, 1040 (1964).
[10] F. Herman and S. Skillman, *Atomic Structure Calculations* (Prentice-Hall, Englewood Cliffs, NJ, 1963).
[11] D. Schaupp *et al.*, J. Phys. Chem. Ref. Data **12**, 467 (1983).
[12] J. H. Hubbell *et al.*, J. Phys. Chem. Ref. Data **4**, 471 (1975).
[13] J. H. Hubbell and I. Overbo, J. Phys. Chem. Ref. Data **8**, 69 (1979).
[14] J. Wang, R. O. Esquivel, V. H. Smith, Jr., and C. F. Bunge, Phys. Rev. A **51**, 3812 (1995).
[15] E. M. A. Peixoto, C. F. Bunge, and R. A. Bonham, Phys. Rev. **181**, 322 (1969).
[16] H. Meyer, T. Müller, and A. Schweig, Chem. Phys. **191**, 213 (1995); Acta Crystallogr. Sect. A **51**, 171 (1995).
[17] E. O. Wollan, Phys. Rev. **37**, 862 (1931).
[18] D. R. Chipman and L. D. Jennings, Phys. Rev. **132**, 728 (1963).
[19] G. E. Ice, M. H. Chen, and B. Crasemann, Phys. Rev. A **17**, 650 (1978).
[20] F. Smend and H. Czerwinski, Z. Phys. D **1**, 139 (1986).
[21] R. Ali *et al.*, Phys. Rev. A **55**, 994 (1997).
[22] F. Biggs, L. B. Mendelsohn, and J. B. Mann, At. Data Nucl. Data Tables **16**, 201 (1975).
[23] Results within the MFF + ASF approximation for Rayleigh scattering are available at "http://www-phys.llnl.gov/V_Div/scattering/elastic.html". S-matrix results are also available on a fixed energy grid.
[24] M. Gavrila, Phys. Rev. A **6**, 1348 (1972); **6**, 1360 (1972); Rev. Roum. Phys. **19**, 473 (1974); A. Costescu and M. Gavrila, Rev. Roum. Phys. **18**, 493 (1973).
[25] P. Eisenberger and P. M. Platzman, Phys. Rev. A **2**, 415 (1970); B. J. Bloch and L. B. Mendelsohn, Phys. Rev. A **9**, 129 (1974); **12**, 551 (1975).